UDC 621.396.96:629.7.01
DOI: 10.15587/2706-5448.2026.353043

Anatoliy Popov,
Iurii Vorobiov,
Kateryna Maiorova,
Mariya Bortsova

ENHANCEMENT OF THE MEASUREMENT METHOD FOR THE RADAR CROSS SECTION OF UNMANNED AERIAL VEHICLES IN THE X-BAND UNDER ANECHOIC CHAMBER CONDITIONS

The object of research is the process of measuring the effective scattering surface of an unmanned aerial vehicle (UAV) in the X-band of electromagnetic waves in an anechoic chamber. The problem being solved is to obtain reliable initial data for assessing the radar visibility and probability of detecting UAVs based on their backscatter diagrams. The aim of research is to improve the method of measuring the effective scattering surface (ESS) of UAV components in the X-band in an anechoic chamber and its experimental testing. As a result of the research, a technology for measuring the angular dependence of the ESS in the X-band was formed, which includes compensation of the background signal, calibration of the measuring equipment, ESS determination of the object and automation of the measurement process. The technology includes the design of the anechoic chamber, the structure of the measuring stand, the method of compensation of the background reflection, measurement of the reflected signal power, calibration of the measuring equipment, ESS calculation. The conducted field experiments allowed to obtain the characteristics of the secondary scattering of UAV components in the angle sector ±45°, while the measurement error of static reference objects did not exceed ±1 dB. Comparison of experimental results with the data of mathematical modeling based on integral equations and the physical theory of diffraction confirmed the reliability of the improved approach. The obtained results can be used to increase the accuracy of assessing the radar visibility of small-sized UAVs and improve the means of their detection.

Keywords: *unmanned aerial vehicle (UAV), radar cross section (RCS), effective scattering surface, backscatter pattern measurement, anechoic chamber.*

Received: 23.11.2025
Received in revised form: 05.02.2026
Accepted: 25.02.2026
Published: 28.02.2026

© The Author(s) 2026
This is an open access article under the Creative Commons CC BY license https://creativecommons.org/licenses/by/4.0/

How to cite
Popov, A., Vorobiov, I., Maiorova, K., Bortsova, M. (2026). Enhancement of the measurement method for the radar cross section of unmanned aerial vehicles in the X-band under anechoic chamber conditions. Technology Audit and Production Reserves, 1 (1 (87)), 15–22. https://doi.org/10.15587/2706-5448.2026.353043

1. Introduction

The growth of the range of unmanned aerial vehicles (UAVs) and their widespread use in reconnaissance, monitoring and special missions necessitates the need to increase the accuracy of assessing their radar visibility [1, 2]. UAVs have become one of the key elements of modern military operations, which determines the relevance of research in the field of their detection and counteraction [3–5].

One of the basic parameters that determines the ability of radar equipment to detect and track UAVs is the effective scattering surface (*ESS*). *ESS* characterizes the intensity of the secondary electromagnetic radiation of an object in response to external radiation and is widely used as a quantitative measure of radar visibility [6]. Methods for measuring and interpreting *ESS* are a fundamental direction of radar research and are discussed in detail in classical works [7, 8].

Experimental methods for determining the *ESS* in the X-band are of particular relevance, since this range is widely used in modern radar systems for surveillance and recognition of small air targets [9–11]. Modern approaches to measuring the EPR of UAVs in flight conditions and in the X-band confirm the need to obtain reliable experimental backscatter diagrams [12].

Carrying out measurements in controlled conditions of an anechoic chamber allows to minimize the influence of external interference and parasitic reflections, but requires special procedures for compensation of the background signal and calibration of measuring equipment [13]. Additionally, the issues of automating measurement procedures in anechoic chambers are important [14].

The object of research is the process of measuring the effective scattering surface of UAVs in the X-band of electromagnetic waves in an anechoic chamber.

The aim of research is to improve the method for measuring the *ESS* of UAV components in the X-band in anechoic chamber conditions.

To achieve the aim, the following objectives were defined:

- to determine the stages of improving the method of measuring the *ESS* of UAV components in the X-band in anechoic chamber conditions;
- to calibrate the measuring stand and estimate the error of experimental measurements of the *ESS* of UAV components;
- to conduct full-scale studies of UAV components in anechoic chamber and compare the obtained results with the data of mathematical modeling.

ISSN-L 2664-9969; E-ISSN 2706-5448

The obtained results can be used to increase the accuracy of assessing the radar visibility of UAVs, as well as to verify digital scattering models in the development of promising radar surveillance systems [10, 15].

2. Materials and Methods

To calculate the radar characteristics of unmanned aerial vehicles, the electrodynamic modeling method was used, which is based on integral representations of classical electrodynamics and short-wave asymptotics, as well as on mathematical methods for determining the angular dependence of the EPR [16]. Unlike classical high-frequency approaches [17], this method allowed to take into account the main mechanisms of radio wave scattering that arise when objects of complex geometric shape are irradiated in the presence of both smooth and edged surface areas, as well as non-ideally reflective fragments and re-reflections between structural elements.

To ensure reliable experimental determination of the *ESS* of UAV components in the X-band under anechoic chamber conditions, the *ESS* measurement method was applied, which was improved by the authors by compensating for the background signal, calibrating the measuring stand using reference objects, and constructing angular backscattering diagrams.

For experimental studies, an anechoic chamber of the National Aerospace University "Kharkiv Aviation Institute" was used, designed for radio engineering measurements, in particular for determining the ESS of small objects in the frequency range of 8–12 GHz [14]. The chamber is located in a closed room and has dimensions of 2.5 × 2.5 × 4.5 m. The volume of the anechoic zone is about 1 m^3 (Fig. 1). The walls, floor and ceiling of the chamber have a grounded metal coating, onto which is glued a radio-absorbing material of the interference-absorbing type [18] based on foam glass with a finely dispersed ferrite filler.

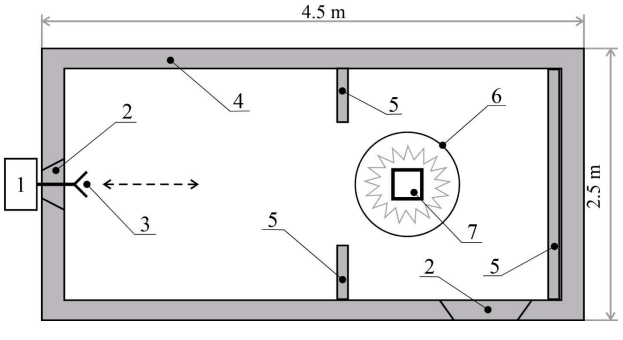

Fig. 1. Plan of an anechoic chamber for *ESS* measurements:
1 – receiver-transmitter; 2 – technological opening; 3 – antenna unit;
4 – radio-absorbing material; 5 – adjustable diaphragms; 6 – anechoic zone;
7 – measurement object

The receiving and measuring equipment was placed outside the chamber. A technological slot was provided in the end for inserting antennas, and in the side wall – an opening for entering the working area and installing research objects. When performing precision measurements, the entrance was closed with a door, also covered with radio-absorbing material.

Adjustable diaphragms were installed inside the chamber, which provide an anechoic zone with a volume of about 1 m^3 at a distance of 3 m from the measuring antennas. The general view of the anechoic chamber is shown in Fig. 2.

The object of measurement was suspended on threads from the ceiling of the chamber at the same level as the receiving and transmitting antennas. The suspension ensured fixation of the object's position and its uniform rotation in the horizontal plane by 360° using a stepper motor with a gearbox controlled by a computer. In this case, 45 measurements of the amplitude of the reflected signal per 1° were performed (a total of 16,000 measurements per full cycle).

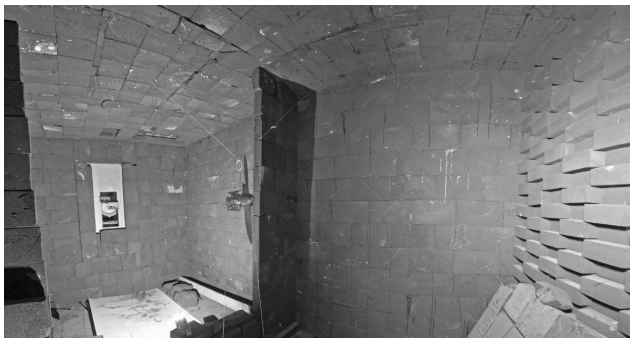

Fig. 2. General view of the anechoic chamber

An automated stand was used to measure the *ESS*, the structure of which is shown in Fig. 3.

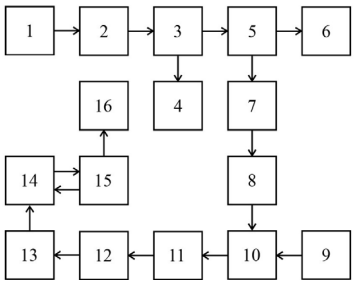

Fig. 3. Structure of the experimental stand for *ESS* measurement:
1 – power supply stabilizer; 2 – microwave generator; 3 – calibrated directional coupler; 4 – power meter; 5 – directional coupler; 6 – transmitting antenna; 7 – adjustable attenuator; 8 – adjustable phase shifter; 9 – receiving antenna; 10 – microwave adder; 11 – detector; 12 – amplifier; 13 – analog-to-digital converter; 14 – computer; 15 – microcontroller; 16 – drive for the device for rotating the measurement object

The formation of the probe microwave signal was carried out by a generator with an operating frequency range of 9–11 GHz and an output power of at least 10 mW. The operating frequency of the transmitter was 9.37 ± 0.01 GHz, the operating mode was continuous. Power control was carried out by the M3-41 meter.

The signal was emitted by a horn antenna with linear polarization. The rotary mechanism provided a change in the polarization orientation angle by 360° with an accuracy of ±0.5°. The level of cross-polarization radiation did not exceed –20 dB. The reflected signal was received by a horn antenna of vertical or horizontal polarization. It is possible to connect a second orthogonally polarized reception channel.

A compensation channel was implemented to compensate for background reflections of the anechoic chamber and the parasitic signal of direct penetration. Part of the transmitter power was fed through an attenuator and a phase shifter to the microwave combiner, which allowed to achieve a minimum signal at the receiver input.

A set of design and technological measures (adjustment of absorption diaphragms, adjustment of the compensation channel, etc.) provided an equivalent "visible EPR" of the camera of no more than 10^{-3} m^2 in the frequency range of 9.3–9.5 GHz.

The amplitude detector is implemented on a mixing diode D405. Since the dependence of the diode current on the signal power is exponential, a logarithmic amplifier is used in the receiver to linearize the characteristic (Fig. 4).

This ensured a dynamic range of the received signals of at least 30 dB. The output signals of the receiver in the range of ±5 V were converted into a digital code by a 16-bit analog-to-digital converter AD976 and transmitted to the computer via the USB interface.

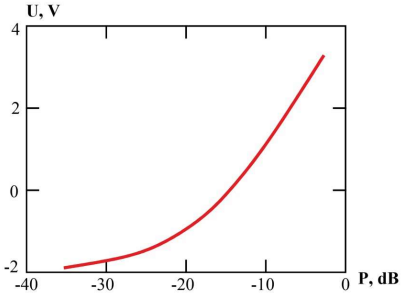

Fig. 4. Dependence of the output voltage *U* of the receiver on the power *P* of the signal

The spatial position of the object was changed by a 4-phase stepper motor with 2048 positions per 360°. To accurately set the initial position, a digital compass on the HMC5983 chip was used.

The position of the object was controlled using the AtMega microcontroller. The operator set the rotation angle with an accuracy of 0.1° or the speed of continuous rotation in order to eliminate the "swaying" of the object suspended on thin threads. The general view of the receiving and transmitting unit of the measuring stand is shown in Fig. 5.

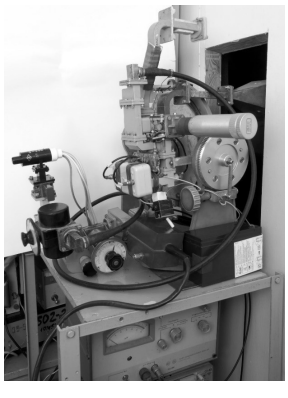

Fig. 5. Appearance of the receiving and transmitting unit of the measuring stand

The unit (Fig. 5) provided the formation of the probing signal, its emission and reception of reflected radiation from the object of research.

To check the operability of the stand and assess the accuracy of measurements, reference metal objects with known theoretical *ESS* values were used. Fig. 6 shows the *ESS* diagrams of a square metal plate 100 × 100 mm, which was used as a calibration object [8, 14].

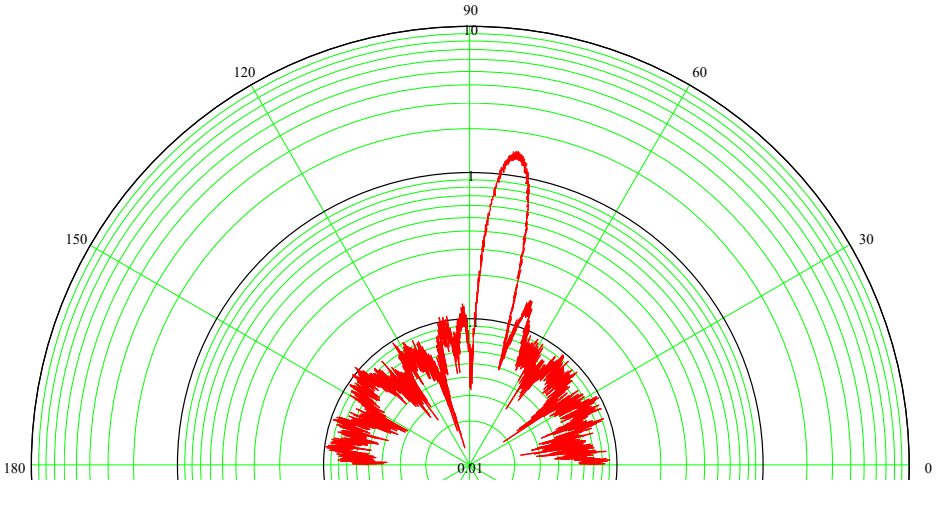

Fig. 6. EPR diagrams of a square metal plate 100 × 100 mm used as a calibration object

3. Results and Discussion

3.1. Stages of improving the method for measuring the effective scattering surface of UAVs in the X-band under anechoic chamber conditions

The general structure of the improved method is shown in Fig. 7.

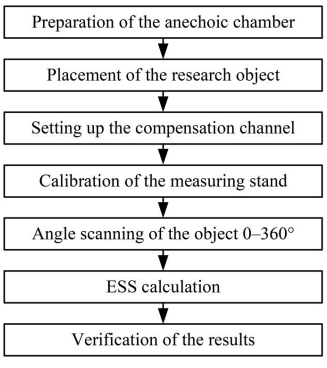

Fig. 7. Block diagram of an improved method for measuring the *ESS* of UAV components in the X-band in an anechoic chamber

Improvement of the method for measuring the effective scattering surface of UAVs in the X-band in an anechoic chamber was implemented in the following sequence of main stages:

1. Preparation of the anechoic chamber and assessment of the level of residual background reflection.
2. Placing the object of research in the anechoic zone and fixing it on the suspension system.
3. Setting up the compensation channel to minimize the parasitic signal of direct penetration and background scattering.
4. Calibration of the measuring stand using reference scatterers with known *ESS* values.
5. Angular scanning of the object within 0–360° with registration of the amplitude of the reflected signal.
6. *ESS* calculation based on the receiver operating characteristic and construction of backscatter diagrams.
7. Verification of results by comparing experimental data with the results of mathematical modeling [16].

3.2. Calibration of the measuring stand and estimation of the error of experimental ESS measurements of UAV components

The dependence of the receiver output voltage *U* on the input signal power is nonlinear (Fig. 4). Therefore, to ensure the accuracy of *ESS* measurements, this characteristic was determined experimentally using a calibrated attenuator with power control by the M3-41 meter with a step of 1 dB. The obtained dependence was approximated by an analytical function of the form

$$P = E_0 + E_1 \cdot C + E_2 \cdot C^2, \qquad (1)$$

where P – the input signal power (dB); E_1 – the approximation coefficients, $i = 0...2$; C – the ADC code.

The function inverse to (1), i. e.

$$C = f(P), \qquad (2)$$

allows the ADC code to determine the power of the input signal. However, this was not enough to directly

ISSN-L 2664-9969; E-ISSN 2706-5448

determine the *ESS* of the research objects without additional calibration calculations.

Since the objects were installed in an anechoic chamber at a fixed distance from the receiving-transmitting unit, measuring reference objects with known *ESS* values made it possible to bind the receiver operating characteristic to the absolute *ESS* values.

Taking into account the fact that the receiver characteristic approximation contains three coefficients E_i, three reference objects with *ESS* that differ significantly from each other (at least by 5–6 dB) were used.

The following were selected as reference objects:

– a ball with a diameter of 99 mm with a calculated *ESS* of $8.6 \cdot 10^{-3}$ m^2;

– a metal pin with a diameter of 5 mm and a length of 198 mm with an *ESS* of $2.8 \cdot 10^{-2}$ m^2;

– a square metal plate (aluminum 1.5 mm) measuring 99 × 99 mm with an *ESS* of 1.4 m^2.

The appearance of the reference objects is shown in Fig. 8.

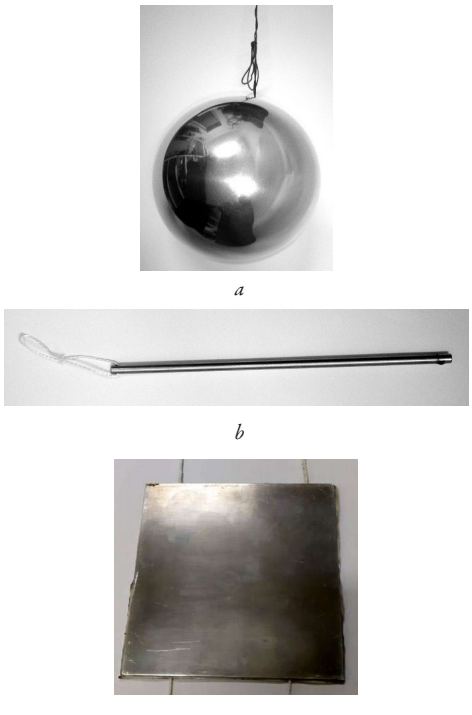

a

b

c

Fig. 8. Reference objects: *a* – ball; *b* – pin; *c* – square plate

According to the results of measurements of signals reflected by reference objects, the approximation coefficients E_i were refined and the operating characteristic of the measuring stand was obtained (Fig. 9). This allowed to move from the measured signal to the ESS numerical value of the UAV component under study.

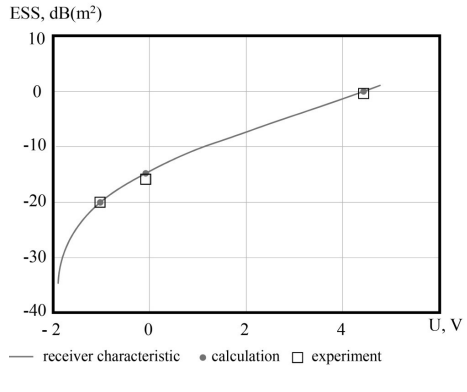

Fig. 9. Binding of the receiver characteristic to reference objects

A comparison of the obtained numerical experimental and calculated values is given in Table 1.

Table 1

Comparison of calculated and experimental data

Object	*ESS*		
	calculation, m^2	calculation, dB	experiment, dB
Square	1.4	1.46	+1.41
Ball	$8.6 \cdot 10^{-3}$	–20.66	–20.8
Pin	$2.8 \cdot 10^{-2}$	–15.53	–16.7

To check the operating characteristics of the stand, a series of square metal plates with dimensions of 80 × 80 mm, 100 × 100 mm, 120 × 120 mm, 140 × 140 mm (Fig. 10) was used, which provides refinement of the measuring scale and reduction of systematic error [14].

Fig. 10. Calibration of the measuring stand using a square plate

The results of the experimental measurement of the maximum *ESS* are given in Table 2 and are graphically presented in Fig. 11.

Table 2

Results of the *ESS* measurement of square plates at a frequency of 9.4 GHz

Object	Theoretical, m^2	Minimum, m^2	Average, m^2	Maximum, m^2
Camera background	0	0.006	0.008	0.014
80 × 80 mm plate	0.57	0.35	0.43	0.53
100 × 100 mm plate	1.40	1.28	1.37	1.45
120 × 120 mm plate	2.89	2.90	3.11	3.17
140 × 140 mm plate	5.3	5.1	5.2	5.22

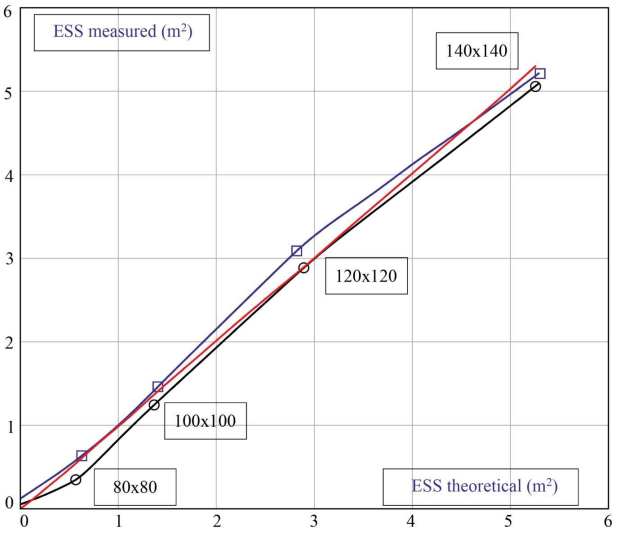

Fig. 11. Dependence of *measured ESS* on *theoretical ESS*: red – theoretical EPR, black – minimum, blue – maximum; point "0" – background level

Thus, the error of *ESS measurement* in the anechoic chamber did not exceed ±1 dB, which is a satisfactory value for conducting field studies of UAV components in the anechoic chamber. It should be noted that for objects with low *ESS*, the systematic error was smaller than for objects with high EPR, which is associated with the nonlinearity of the receiver amplitude characteristic.

3.3. Field studies of UAV components in the anechoic chamber and comparison of the obtained results with the data of mathematical modeling

3.3.1. Metal elements and electronic components of UAV

Taking into account the fact that the greatest contribution to the UAV *ESS* is made by metal elements and electronic components, a mock-up of the UAV control unit was used (Fig. 12). The model of the UAV control unit had the appearance of a rectangular parallelepiped measuring 68 × 90 × 54 mm with a metallized surface.

Fig. 13 shows the results of the calculation of the backscattering diagram of a parallelepiped and experimental measurements of ESS depending on the angle of irradiation.

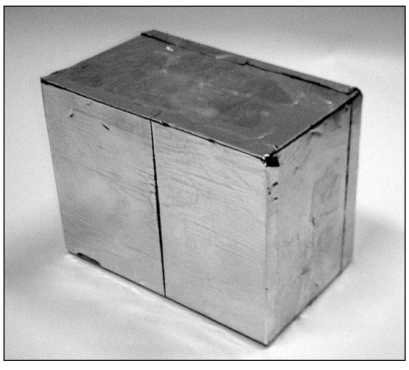

Fig. 12. Layout of the UAV control unit

The results of experiments and calculations are given in Table 3.

Analysis of the data in Table 3 allowed to establish a decrease in the experimental ESS values compared to the calculated ones for the adopted UAV block model (Fig. 12), which may be due to insufficient conductivity of the metallized coating of the object.

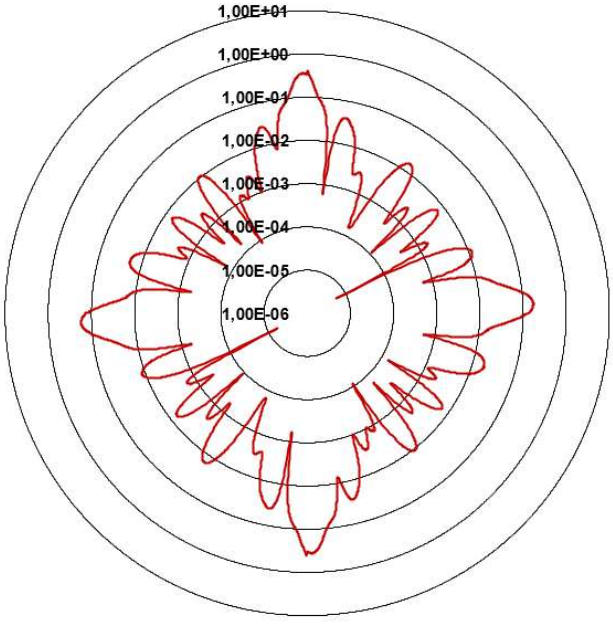

a

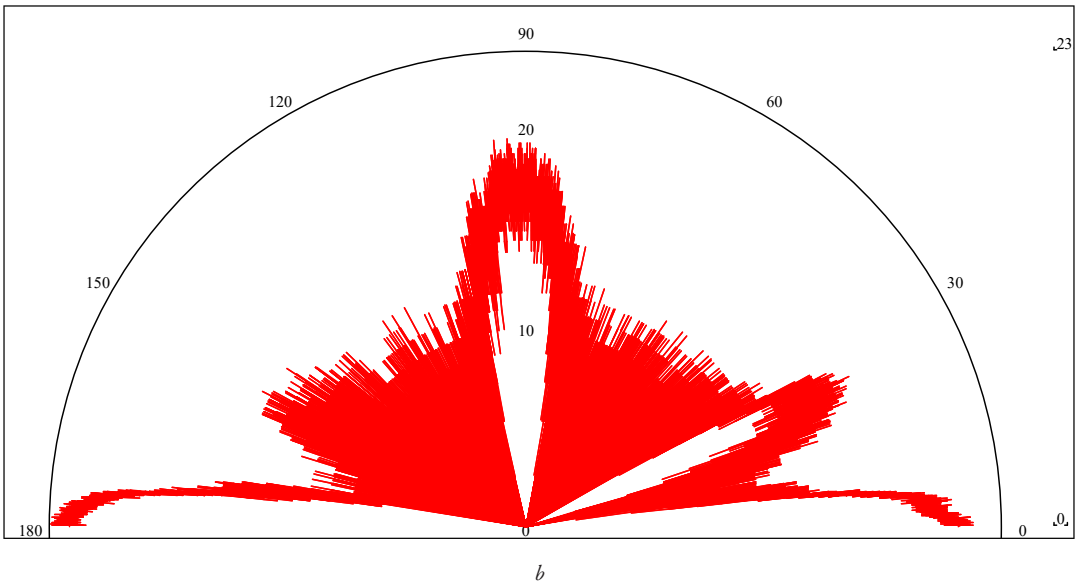

b

Fig. 13. Scattering diagrams of a metallized parallelepiped: *a* – calculation; *b* – measurement

ISSN-L 2664-9969; E-ISSN 2706-5448

Table 3

Comparison of calculated and experimental data for a parallelepiped

Edge	*ESS* (calculation), m^2	*ESS* (calculation), dB	*ESS* (experiment), dB
90 × 68 mm	$4.09 \cdot 10^{-1}$	–3.88	–5.01
68 × 54 mm	$1.59 \cdot 10^{-1}$	–7.99	–10.5

3.3.2. UAV engine

Fig. 14 shows the experimental UAV engine, and Fig. 15 shows the suspension method in the anechoic chamber.

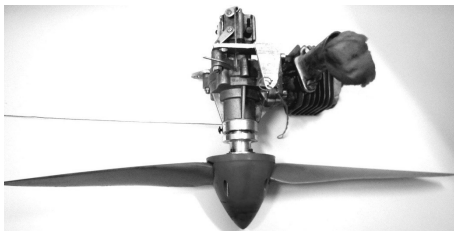

Fig. 14. UAV engine

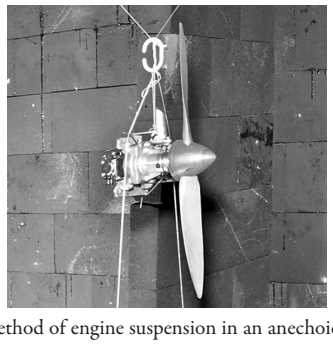

Fig. 15. Method of engine suspension in an anechoic chamber

The measurement results are shown in Fig. 16 and 17.

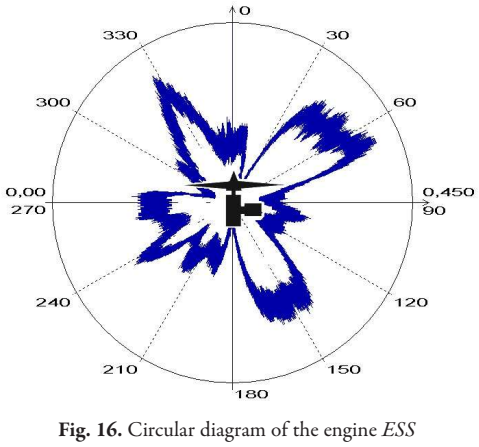

Fig. 16. Circular diagram of the engine *ESS*

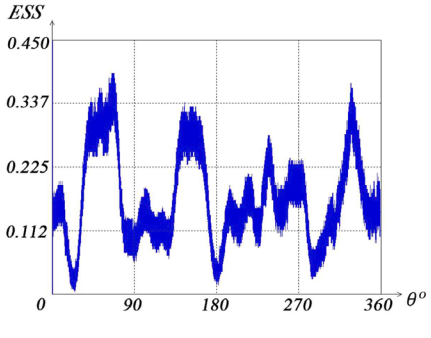

Fig. 17. Dependence of the engine *ESS* on the angle of irradiation

Analysis of the obtained data (Fig. 16, 17) showed that the largest reflections were formed by angular reflectors formed by the engine structural elements. The average *ESS* of the engine was 0.165 m^2 with a standard deviation of 0.077 m^2. The instantaneous *ESS* value varied within wide limits from 0.001 m^2 to 0.45 m^2, i. e. the dynamic range of *ESS* changes exceeded 25 dB. This can lead to disruption of radar tracking of the target when the observation angle changes. The histogram of the distribution of the engine ESS at an equally probable angle of irradiation is shown in Fig. 18.

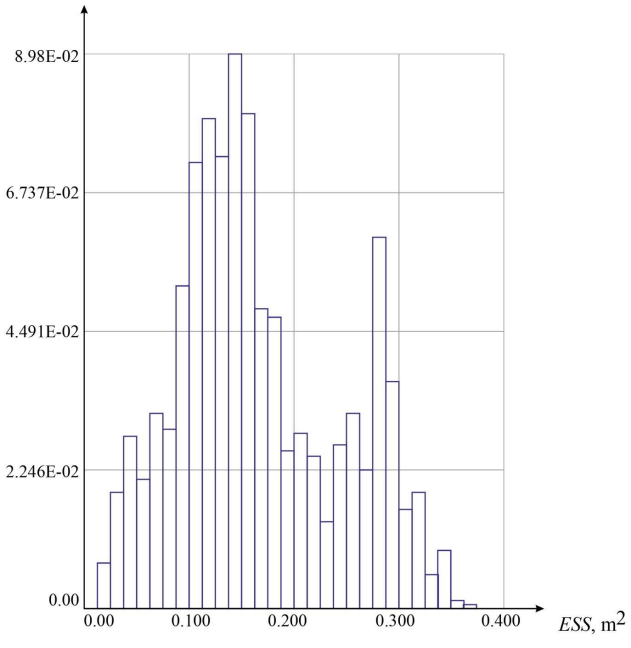

Fig. 18. Histogram of the ESS distribution of the engine

Analysis of the histogram (Fig. 18) showed a median *ESS* value of 0.156 m^2 with an average value of 0.165 m^2. Low ESS values are more likely, which should be taken into account when choosing detection thresholds. Data on the distribution of the average *ESS* by irradiation sectors ±10° are given in Table 4.

Table 4

Distribution of the average EPR by irradiation sectors ±10° for a parallelepiped

Sector No.	Sector, degrees	*ESS*, m^2
1	–10...+10	0.1452
2	+10...+30	0.1247
3	+30...+50	0.2922
4	+50...+70	0.2540
5	+70...+90	0.1032
6	+90...+110	0.1225
7	+110...+130	0.1450
8	+130...+150	0.2773
9	+150...+170	0.1611
10	+170...+190	0.0995
11	+190...+210	0.1435
12	+210...+230	0.1677
13	+230...+250	0.1635
14	+250...+270	0.1835
15	+270...+290	0.0695
16	+290...+310	0.1429
17	+310...+330	0.2587
18	+330...+350 (–10)	0.1478

3.4. Research limitations and prospects for further work

To improve the accuracy of modeling the angular dependences of *ESS*, it is necessary to use geometric data obtained by 3D-scanning of the surfaces of real objects [19].

The results obtained have an applied value for improving the accuracy of determining the backscatter diagrams of UAV structural elements. Experimental data, confirmed by mathematical modeling, create the basis for the development of radar systems for detecting low-visibility UAVs.

The research was performed in an anechoic chamber at a fixed frequency of continuous radiation. Real radars use pulsed broadband or frequency-modulated signals, which was not taken into account within the framework of this experiment. In addition, only two typical components of the UAV were studied, which make the greatest contribution to its *ESS*.

Further research should be directed to:

- expanding the list of research objects, in particular non-metallic ones;
- upgrading the stand for broadband measurements;
- use of noise-like signals;
- use of 3D-scanning data for modeling;
- experimental verification of results for geometrically complex elements of the UAV design.

4. Conclusions

1. Improvement of the method for measuring the *ESS* of UAV components in the X-band in an anechoic chamber is based on the implementation of a block diagram that includes 7 consecutive stages.

2. Calibration of the measuring stand and assessment of the error of experimental measurements of the *ESS* for UAV components were performed. It was established that the measurement error did not exceed ±1 dB, where for objects with a small ESS the systematic error was smaller than for objects with a large *ESS*, which is explained by the nonlinearity of the amplitude characteristic of the receiver.

3. Comparison of the results of full-scale experiments of UAV components in an anechoic chamber with the data of mathematical modeling showed the following. A slight decrease in the experimental *ESS* values was obtained compared to the calculated ones for the adopted UAV block layout, which is explained by the insufficient conductivity of the metallized coating of the object. Analysis of the engine *ESS* distribution histogram data showed low *ESS* values (median EPR value 0.156 m^2 with an average value of 0.165 m^2) as more probable, which should be taken into account when choosing detection thresholds. The dynamic range of *ESS* changes exceeded 25 dB, which should be taken into account when changing the observation angle to prevent disruption of radar tracking of the target.

Conflict of interest

The authors declare that they have no conflict of interest in relation to this research, whether financial, personal, authorship or otherwise, that could affect the research and its results presented in this paper.

Financing

The research was performed without financial support.

Data availability

The manuscript has no associated data.

Use of artificial intelligence

The authors confirm that they did not use artificial intelligence technologies when creating the current work.

Authors' contributions

Anatoliy Popov: analysis of the state of the issue, formulation of the object, goals and objectives of the research, calculation and construction of EPR diagrams of the UAV design; ***Iurii Vorobiov:*** creation of EPR measurement technology of the UAV design, formulation of conclusions; ***Kateryna Maiorova:*** comparison of the obtained results of the full-scale experiment with the data of the mathematical modeling of the UAV; ***Mariya Bortsova:*** collection, analysis of data and setting up the experiment in an anechoic chamber.

References

1. Zhuk, S., Bilorus, A., Bomberher, V., Lukovskiy, I. (2025). Use of unmanned systems in modern military operations: analysis of efficiency and risks. *Collection of Scientific Works of the National Academy of the State Border Guard Service of Ukraine. Series: Military and Technical Sciences, 99 (2),* 4–14. https://doi.org/10.32453/3.v99i2.1882
2. Vorobiov, Yu., Maiorova, K., Popov, A., Diachenko, Yu., Bezkorovainyi, V. (2025). Development of an ontological decision support system for selection of aircraft-type unmanned aerial vehicles. *Science and technology today, 11 (52),* 1944–1961. https://doi.org/10.52058/2786-6025-2025-11(52)-1944-1961
3. Kovalov, K. (2025). UAVs in the reconnaissance and fire control system: current status and prospects. *International scientific journal "Grail of Science", 55,* 339–345. https://doi.org/10.36074/grail-of-science.22.08.2025.039
4. Bezpilotni systemy ta REB: pidsumky ta dosiahnennia sichnia 2025 roku. *Zbroini Syly Ukrainy.* Available at: https://www.zsu.gov.ua/news/bezpilotni-systemy-ta-reb-pidsumky-ta-dosyagnennya-sichnya-2025-roku
5. Vorobiov, I., Maiorova, K., Sosunov, A. (2026). Methodology for assessing the economic efficiency of using an ontology-based decision support system for selecting aircraft-type unmanned aerial vehicles. *Aerospace Technic and Technology, 1,* 84–94. https://doi.org/10.32620/aktt.2026.1.08
6. Jenn, D. C. (2024). Radar Cross Section. *Encyclopedia of RF and Microwave Engineering,* 1–43. https://doi.org/10.1002/0471654507.erfme058
7. Shevchenko, S. (2025). An improved methodology for determining unmanned aerial vehicles radar visibility characteristics in a model experiment. *Scientific Works of Kharkiv National Air Force University, 4 (82),* 72–82. https://doi.org/10.30748/zhups.2024.82.09
8. Knott, E. F. (1993). *Radar Cross Section Measurements.* New York: Springer. https://doi.org/10.1007/978-1-4684-9904-9
9. Ezuma, M., Anjinappa, C. K., Semkin, V., Guvenc, I. (2022). Comparative Analysis of Radar-Cross-Section- Based UAV Recognition Techniques. *IEEE Sensors Journal, 22 (18),* 17932–17949. https://doi.org/10.1109/jsen.2022.3194527
10. Sukharevsky, O., Zalevsky, G., Vasilets, V., Galkin, Y., Horielyshev, S., Sadovyi, K. (2021). Radar scattering characteristics of tactical unmanned aerial vehicle in VHF, S and X frequency bands. *Science and Technology of the Air Force of Ukraine,, 4 (45),* 82–92. https://doi.org/10.30748/nitps.2021.45.10
11. Surhai, M. V., Zalevskyi, H. S., Vasylets, V. O., Sukharevskyi, O. I. (2017). Otsiniuvannia rivnia radiolokatsiinoi pomitnosti snariadu raketnoi systemy zalpovoho vohniu "Hrad" u riznykh diapazonakh dovzhyn khvyl. *Zbirnyk naukovykh prats Kharkivskoho natsionalnoho universytetu Povitrianykh Syl, 2 (51),* 142–148. Available at: http://nbuv.gov.ua/UJRN/ZKhUPS_2017_2_30
12. Liu, J., Yinchai, W., Wei, F., Han, Q., Tao, Y., Zhao, L. et al. (2023). Secure Cloud-Aided Approximate Nearest Neighbor Search on High-Dimensional Data. *IEEE Access, 11,* 109027–109037. https://doi.org/10.1109/access.2023.3321457
13. Hemming, L. H. (2002). *Anechoic Chamber Design Techniques. Electromagnetic Anechoic Chambers.* Wiley-IEEE Press, 57–72. https://doi.org/10.1109/9780470544501.ch5
14. Popov, A., Kalimullin, D. (2020). Automatization of Antenna Measurements in the Anechoic Chamber. *2020 IEEE Ukrainian Microwave Week (UkrMW).* Kharkiv: IEEE, 183–186. https://doi.org/10.1109/ukrmw49653.2020.9252594
15. Sukharevsky, O. I. (2018). *Electromagnetic Wave Scattering by Aerial and Ground Radar Objects.* CRC Press, 334. https://doi.org/10.1201/9781315214511
16. Zalevsky, G. S., Sukharevsky, O. I., Vasylets, V. A. (2021). Integral equation modelling of unmanned aerial vehicle radar scattering characteristics in VHF to S frequency bands. *IET Microwaves, Antennas & Propagation, 15 (10),* 1299–1309. Portico. https://doi.org/10.1049/mia2.12164
17. Ufimtsev, P. Y. (2014). *Fundamentals of the physical theory of diffraction.* Wiley-IEEE Press, 496. Available at: https://download.e-bookshelf.de/download/0002/4020/78/L-G-0002402078-0003467319.pdf

ISSN-L 2664-9969; E-ISSN 2706-5448

18. Panwar, R., Puthucheri, S., Singh, D. (2018). Experimental Demonstration of Novel Hybrid Microwave Absorbing Coatings Using Particle-Size-Controlled Hard–Soft Ferrite. *IEEE Transactions on Magnetics, 54 (11),* 1–5. https://doi.org/10.1109/tmag.2018.2828782

19. Zhao, H., Chen, J., Zhuang, M., Yang, X., Zhuo, J. (2024). A Novel Radar Cross-Section Calculation Method Based on the Combination of the Spectral Element Method and the Integral Method. *Symmetry, 16 (5),* 542. https://doi.org/10.3390/sym16050542

Anatoliy Popov, *Doctor of Technical Sciences, Associate Professor, Department of Aerospace Radioelectronic Systems, National Aerospace University "Kharkiv Aviation Institute", Kharkiv, Ukraine, ORCID: https://orcid.org/0000-0003-0715-3870*

✉ ***Iurii Vorobiov,*** *Doctor of Technical Sciences, Professor, Department of Aircraft Manufacturing Technology, National Aerospace University "Kharkiv Aviation Institute", Kharkiv, Ukraine, e-mail: i.vorobiov@khai.edu, ORCID: https://orcid.org/0000-0001-6401-7790*

Kateryna Maiorova, *PhD, Associate Professor, Department of Aircraft Manufacturing Technologies, National Aerospace University "Kharkiv Aviation Institute", Kharkiv, Ukraine, ORCID: https://orcid.org/0000-0003-3949-0791*

Mariya Bortsova, *Air Force Research Center, Ivan Kozhedub Kharkiv National Air Force University, Kharkiv, Ukraine, ORCID: https://orcid.org/0000-0001-6644-0875*

✉ *Corresponding author*